PHYSICAL REVIEW FLUIDS **2**, 052001(R) (2017)

Fast inertial particle manipulation in oscillating flows

Raqeeb Thameem,[1] Bhargav Rallabandi,[2] and Sascha Hilgenfeldt[1,*]

[1]*Department of Mechanical Science and Engineering, University of Illinois at Urbana-Champaign, Urbana, Illinois 61801, USA*

[2]*Department of Mechanical and Aerospace Engineering, Princeton University, Princeton, New Jersey 08544, USA*

(Received 21 October 2016; published 3 May 2017)

It is demonstrated that micron-sized particles suspended in fluid near oscillating interfaces experience strong inertial displacements above and beyond the fluid streaming. Experiments with oscillating bubbles show rectified particle lift over extraordinarily short (millisecond) times. A quantitative model on both the oscillatory and the steady time scales describes the particle displacement relative to the fluid motion. The formalism yields analytical predictions confirming the observed scaling behavior with particle size and experimental control parameters. It applies to a large class of oscillatory flows with applications from particle trapping to size sorting.

DOI: 10.1103/PhysRevFluids.2.052001

The manipulation of particles in microfluidic flows is a central task in manifold applications in laboratory-on-a-chip or biomedical applications [1]. Passive transport in the flow is not sufficient if microparticles such as biological cells are supposed to be displaced, trapped, or sorted according to size or other physical properties. Recently, inertial forces on particles have been discussed prominently for such purposes, including slow displacement by the action of shear gradients [2–4] or more rapid motion in acoustofluidics [5–8]. We here describe a form of inertial manipulation of particles close to oscillating interfaces, effecting fast actuation without relying on the acoustofluidic requirements of density or compressibility contrast between the particle and fluid.

Few experiments have detailed the displacement of particles in periodic flows driven from moving boundaries. Particle rearrangement in vibrating containers [9–11], object capture in streaming vortices [12], or trapping by radiation forces [13,14] have been reported, and studies with oscillating bubbles demonstrate differential deflection over short time and length scales [15,16]. However, a rigorous understanding of the particle trajectories in these flows and the underlying physical principles is missing.

Oscillatory fluid motion in general gives rise to steady streaming flow, which has great practical relevance in applications [17,18]. While the experiments described here feature bubble microstreaming, it should be stressed that both the oscillatory and the streaming flow are fully known analytically and described in previous work [19,20], and that the streaming flow is merely utilized to guide the particles into the vicinity of the oscillating interface. The current Rapid Communication focuses entirely on particle displacements beyond passive fluid element motion.

A schematic of a typical bubble microstreaming device design is shown in Fig. 1(a) (cf. Refs. [15,16,19]). A blind side channel off a polydimethylsiloxane (PDMS) microchannel traps a semicylindrical air bubble of radius $a_b = 40\ \mu$m. The device is bonded to a glass slide with a piezoelectric transducer (Physik Instrumente) driven through a function generator (model 7075, Hioki) and an amplifier (model 7500, Krohn-Hite) at frequencies $f = \omega/(2\pi) = 20$–40 kHz. The resulting bubble oscillations have a small amplitude $\epsilon \ll 1$ (normalized by a_b) and excite both a primary, oscillatory flow $\mathbf{u}_0$ and a secondary, steady streaming flow $\mathbf{u}_s$ [see Fig. 1(b)]. The velocity scales of these flows are $u_0 = \epsilon a_b \omega$ and $u_s = \epsilon^2 a_b \omega$, respectively [21,22]. Syringe pumps (PHD Ultra, Harvard Apparatus and EW-74905, Cole-Parmer) establish constant equal flow rates through

*sascha@illinois.edu

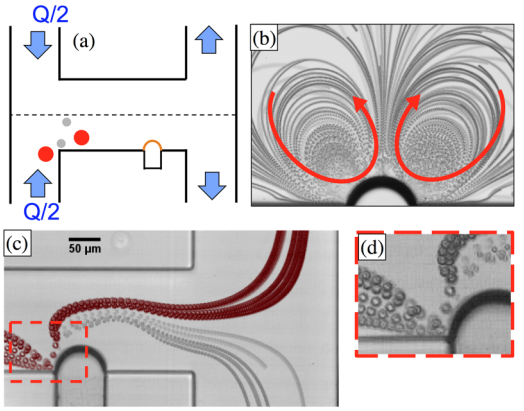

FIG. 1. (a) Schematic of device design for sorting: The upper inlet flow carries fluid only, while flow from the lower inlet carries particles. (b) Characteristic vortex pair streaming flow around a bubble, visualized by passive tracers. (c) Streak image of separation of $a_p = 2.5\ \mu$m particles (gray) and $a_p = 5\ \mu$m particles (red); the flow is a superposition of streaming and transport flow. (d) Closeup near the bubble interface: Differential particle deflection happens rapidly and locally and is quantified in the present work.

both inlets [Fig. 1(a)], superimposing a transport flow onto the bubble-driven flow. Polystyrene microparticles of radius $a_p = 0.5$–$5\ \mu$m are introduced through only one of the inlets into the density-matched fluid (24% glycerol/water w/w; kinematic viscosity $\nu \approx 2 \times 10^{-6}$ m^2/s). The combined flow ensures that the particles are transported near the bubble, where they are separated by size reliably with high throughput [16]. In Fig. 1(c), particles of $a_p = 5\ \mu$m are deflected into the opposite outlet, while those with $a_p = 2.5\ \mu$m remain in the lower half of the device.

Clearly, particles experience size-dependent differential deflection (lift) across streamlines; a closeup [Fig. 1(d)] shows that all deflections happen over very short times ($\sim$1 ms) very close to the bubble surface. The process has been semiquantitatively described as a hard-core steric interaction between particles and bubble [16], but in the present experiments we observe particle dynamics in detail with a high-speed camera (Phantom v310, Vision Research) and find this explanation insufficient.

Figure 2(a) shows the trajectories of two particles near a bubble, resolved at 100 000 fps. Direct inspection of the movie (see the Supplemental Material [23]) confirms that the particles are never in contact with the bubble surface, but are gradually displaced radially outwards while simultaneously performing oscillations. The displacement of the larger particle is markedly greater. The observation

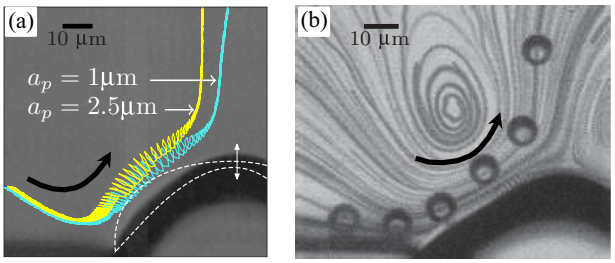

FIG. 2. (a) Experimental trajectories of two particles, taken at 100 000 fps frame rate. Initially at very similar positions, the particles oscillate with the bubble motion (extreme positions of the oscillating bubble outline are indicated as dashed lines), but are never in contact with the bubble interface. Over several cycles, particles are displaced outward, with larger particles experiencing greater deflection. (b) Snapshots from a stroboscopic movie, with streaks from small passive tracers ($a_p = 0.5\ \mu$m) providing a background for the motion of a large particle ($a_p = 5\ \mu$m, six positions indicated).

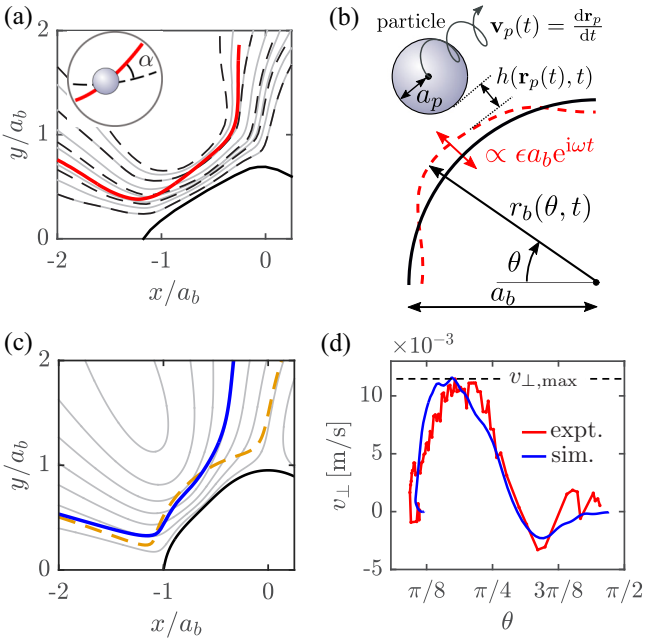

FIG. 3. (a) Experimental trajectory of the large particle from Fig. 2(b) on the background of proxy streamlines (dashed; gray lines are interpolations), showing strong lift displacements (large angles α) close to the bubble surface. (b) Schematic and nomenclature for a quantitative description of the particle trajectory $\mathbf{r}_p(t)$. (c) Stroboscopic trajectory (blue) from solving (3), with fluid pathlines indicated as gray lines. The orange, dashed line is a computed particle trajectory without oscillatory flow, which shows negligible net displacement. (d) Particle velocity component $v_\perp$ perpendicular to streamlines as a function of the azimuthal angle θ along the trajectory in experiment (red) and simulation (blue), showing good agreement throughout; the peak value $v_{\perp,\max}$ is indicated.

is consistent with the hydrodynamic expectation of a thin fluid layer between the particle and bubble hindering surface-to-surface contact [24,25].

Note that the particle Reynolds number associated with the steady motion component (at typical $\epsilon \lesssim 0.1$, $\mathrm{Re}_p^{(s)} = u_s a_p/\nu \ll 1$) is a factor ϵ smaller than that of the oscillatory flow ($\mathrm{Re}_p^{(0)} = u_0 a_p/\nu \gtrsim 1$ for $a_p \gtrsim 2\ \mu$m). Therefore, an understanding of any inertial effects behind the observed lift must include the primary oscillatory flow.

Lift displacements of particles can be quantified more accurately by analyzing the movies stroboscopically: Imaging one frame per driving cycle in an experiment with one $a_p = 5\ \mu$m particle ($\mathrm{Re}_p^{(0)} > 1$) amidst a large number of $a_p = 0.5\ \mu$m particles ($\mathrm{Re}_p^{(0)} \ll 1$), the latter's trajectories provide proxies for fluid pathlines (we will show below that the lift on these small particles is negligible). Figure 2(b) shows snapshots of the large particle superimposed on streaks of the small particle flow pattern, while Fig. 3(a) shows the extracted large-particle path. At points of intersection between the large-particle trajectory and proxy streamlines (including interpolations between small-particle trajectories), we measure both the steady particle speed $|\mathbf{v}_s|(t)$ and the angle of intersection $\alpha(t)$ [cf. Fig. 3(a)]. The particle velocity normal to the streamline is $v_\perp = |\mathbf{v}_s| \sin\alpha$, and is a direct quantitative measure of local deflection across streamlines.

We find that, independent of the oscillation phase chosen for stroboscopic imaging, $v_\perp$ reaches its peak value near the location at which the particle is closest to the bubble surface; cf. Fig. 3(d) for a typical result. We denote $v_{\perp,\max}$ as the maximum of this peak value over all phases for a single-particle trajectory. This experimental procedure was carried out for dozens of particles over several driving voltages (changing ϵ), driving frequencies ω, and two large-particle sizes ($a_p = 5\ \mu$m

and $a_p = 2.5\ \mu$m). All results confirm the rapid lift displacement of the particles near the bubble, and a strong increase in displacement with particle size. The duration of appreciable lift [large $v_\perp(t)$] is typically 10–20 oscillation cycles (0.5–1 ms).

Considering the unusually fast and specific application of forces in this microfluidic device, it is desirable to have a quantitative understanding of the displacement process. Modeling is aided by the available analytical results for the bubble streaming flow field [19,20] and the superimposed transport flow [16]. The Maxey-Riley (MR) equation [26] provides a conceptually straightforward description of particle dynamics in free space and involves a balance between the hydrodynamic forces, inertia (both particle and fluid), and the momentum diffusion away from the particle (the Boussinesq-Basset history force). For the parameters of the present system, Faxén contributions are small to relative order $(a_p/a_b)^2$ and can be neglected; we also neglect the history term, a simplification which can be shown to be self-consistent (see Supplemental Material [23]). The MR equation is then

$$2\pi a_p^3 \rho \left(\frac{d^2 \mathbf{r}_p}{dt^2} - \frac{D\mathbf{u}}{Dt} \right) = \mathbf{F}_H, \tag{1}$$

where D/Dt is the material time derivative and $\mathbf{r}_p(t)$ is the position of the particle center. An important modification to the free-space MR equation is due to the varying distance of the particle to the oscillating bubble interface. For large distances, the hydrodynamic force is simply the Stokes drag $\mathbf{F}_H^\infty = -6\pi\eta a_p (\mathbf{v}_p - \mathbf{u})_{\mathbf{r}_p}$, where $\mathbf{v}_p = d\mathbf{r}_p/dt$ is the instantaneous particle velocity. Conversely, for a particle close to the stress-free bubble, the force is given by lubrication theory as $\mathbf{F}_H^{\text{lub}} = -6\pi\eta a_p^2 \mathbf{e}_r (\mathbf{v}_p \cdot \mathbf{e}_r - \partial_t r_b)/(4h)$, which is valid in the limit $h \ll a_p \ll a_b$ [24,27] for small-amplitude oscillations ($\epsilon \ll 1$) of the bubble from its mean circular position [Fig. 3(b)]. Here, $r_b(\theta,t)$ is the radial position of the oscillating interface and $h(\mathbf{r}_p,t)$ is the separation distance between the surfaces of the particle and the bubble—see Fig. 3(b) for the nomenclature. While a rigorous expression for $\mathbf{F}_H$ for all distances can be derived [24,28], it is convenient (in the spirit of Ref. [29]) to superpose the two limits ($\mathbf{F}_H \approx \mathbf{F}_H^\infty + \mathbf{F}_H^{\text{lub}}$), obtaining

$$\mathbf{F}_H \approx -6\pi\eta a_p \left\{ \frac{d\mathbf{r}_p}{dt} - \mathbf{u} + \frac{a_p \left(\frac{d\mathbf{r}_p}{dt} \cdot \mathbf{e}_r - \frac{\partial r_b}{\partial t} \right)}{4h(\mathbf{r}_p,t)} \mathbf{e}_r \right\}_{\mathbf{r}_p}, \tag{2}$$

which remains asymptotically accurate (to leading order) for both large and small particle-bubble separations [24,25,30].

Defining dimensionless variables $\tilde{\mathbf{r}} = \mathbf{r}/a_b$, $\tilde{t} = \omega t$, and $\tilde{\mathbf{u}} = \mathbf{u}/u_0$, (1) and (2) yield a modified Maxey-Riley equation for the particle position $\tilde{\mathbf{r}}_p(t)$,

$$\lambda \frac{d^2 \tilde{\mathbf{r}}_p}{d\tilde{t}^2} + \left(\mathbf{I} + \frac{\gamma\, \mathbf{e}_r \mathbf{e}_r}{\tilde{h}(\tilde{\mathbf{r}}_p,t)} \right) \cdot \frac{d\tilde{\mathbf{r}}_p}{d\tilde{t}} - \epsilon \left\{ \lambda \left(\frac{\partial \tilde{\mathbf{u}}}{\partial \tilde{t}} + \epsilon\, \tilde{\mathbf{u}} \cdot \tilde{\nabla} \tilde{\mathbf{u}} \right) + \tilde{\mathbf{u}} + \frac{\gamma}{\tilde{h}(\tilde{\mathbf{r}},t)} \frac{\partial \tilde{r}_b}{\partial \tilde{t}} \mathbf{e}_r \right\}_{\tilde{\mathbf{r}}_p} = \mathbf{0}, \tag{3}$$

where $\tilde{h}(\tilde{\mathbf{r}}_p,t) = \tilde{r}_p - \tilde{r}_b - 4\gamma$ is the dimensionless particle-bubble separation distance. Furthermore,

$$\lambda = \frac{a_p^2 \omega}{3\nu} \quad \text{and} \quad \gamma = \frac{a_p}{4a_b} \tag{4}$$

are, respectively, the dimensionless particle inertia and a ratio of length scales of the particle and the boundary.

Equation (3) is an ordinary differential equation for the trajectory $\tilde{\mathbf{r}}_p(\tilde{t})$ of the particle that depends on λ, γ, and the amplitude $\epsilon \ll 1$. The fluid velocity field can be expanded as

$$\tilde{\mathbf{u}}(\tilde{\mathbf{x}},\tilde{t}) = \tilde{\mathbf{u}}_0(\tilde{\mathbf{x}}) e^{i\tilde{t}} + \epsilon \tilde{\mathbf{u}}_1(\tilde{\mathbf{x}}) \cdots, \tag{5}$$

where $\tilde{\mathbf{u}}_0 e^{i\tilde{t}}$ is the oscillatory velocity and $\tilde{\mathbf{u}}_1$ is the steady flow comprising both the steady bubble streaming $\mathbf{u}_s$ and the channel transport flow. The two-dimensional (2D) geometry of the problem allows for a closed-form derivation of $\tilde{\mathbf{u}}(\tilde{\mathbf{x}})$ at a given driving frequency and amplitude [16,19,20];

deviations from 2D flow can be important for vortex-trapped particles over very long time scales [31,32], but are unimportant for this modeling of fast displacements.

We stress that this formalism takes into account the full geometry and dynamics of the moving interface as well as its effect on the flow field. Thus it differs from approaches using lubrication terms in a Lattice-Boltzmann setting with an imposed cutoff [33] or introducing Saffman lift [34] (a term sensitive to local gradients in the flow, and strictly applicable only in situations where there are no fluid boundaries near the particle).

A numerical solution of (3) provides a direct comparison with experiment, from which we extract initial conditions (position and velocity) for the particle, as well as the values of all physical parameters. The simulations (which give results on the oscillatory as well as steady time scales) are analyzed exactly as the experiments: Particle positions are registered once per cycle and the particle drift velocity $v_\perp(t)$ inferred. Figure 3(c) shows the resulting stroboscopic trajectory and displacement of the particle. Also shown (dashed) is a trajectory computed with the oscillatory part of the flow field omitted (by setting $\tilde{\mathbf{u}}_0 = \mathbf{0}$ and $\partial \tilde{r}_b/\partial t = 0$), confirming that particle inertia in the steady flow is too small to lead to an appreciable net drift of the particle position across streamlines.

A direct comparison of the perpendicular particle velocity $v_\perp$ obtained from the model to experiment in Fig. 3(d) shows excellent agreement—we stress that this plot is not a fit, with all modeling parameters directly obtained from experiment. To gain more insight into how the particle trajectories change with the experimental parameters, we perform a further analytical simplification of the modified MR equation (3). While the oscillatory part of the dynamics is generally a combination of a radial monopole mode and surface modes of smaller amplitude [19], we shall assume that the latter are only important in establishing the streaming flow but are otherwise negligible, so that we can replace $\tilde{\mathbf{u}}$ by

$$\tilde{\mathbf{u}}(\tilde{\mathbf{x}}) \approx \tilde{\mathbf{u}}_0^M e^{i\tilde{t}} + \epsilon \tilde{\mathbf{u}}_L(\tilde{\mathbf{x}}). \tag{6}$$

Here, the oscillatory flow is governed by the monopole $\tilde{\mathbf{u}}_0^M(\mathbf{x}) = \mathbf{e}_r/\tilde{r}$, and the steady flow is taken to be the Lagrangian velocity field $\tilde{\mathbf{u}}_L(\mathbf{x})$ obtained from the full analytical expression, which by definition makes the time-averaged fluid trajectories identical in the full and simplified formulations (see Supplemental Material [23]). Consistent with this approximation, the interface shape is now $\tilde{r}_b \approx 1 - i\epsilon\, e^{i\tilde{t}}$. Note that $\tilde{\mathbf{u}}_L \cdot \mathbf{e}_r|_{\tilde{r}=1} = 0$, as average fluid trajectories do not penetrate the mean bubble interface. The azimuthal motion of the particle is then steady and follows $\tilde{\mathbf{u}}_L \cdot \mathbf{e}_\theta$ passively, while particle deflections follow from the radial component of (3).

We observe that the flow has two well-separated time scales, a fast oscillatory scale $\tilde{t}$, and a slow steady scale $\tilde{T} = \epsilon^2 \tilde{t}$, which is a characteristic transport time set by the steady flow (a_b/u_s in dimensional terms). We seek a solution for the particle motion in the form

$$\tilde{\mathbf{r}}_p(\tilde{t}, \tilde{T}) = \tilde{\mathbf{r}}_{p0}(\tilde{T}) + \epsilon\, \tilde{r}_{p1}(\tilde{T})\, e^{i\tilde{t}}\, \mathbf{e}_r + \cdots, \tag{7}$$

where $\tilde{\mathbf{r}}_{p0}(\tilde{T})$ represents the 2D steady trajectory of the particle and $\epsilon \tilde{r}_{p1}(\tilde{T})$ is its radial oscillation amplitude along its trajectory. Solving (3) perturbatively for $\epsilon \ll 1$ using standard techniques of time-scale separation [35], we find that a particle follows the fluid oscillation with a phase shift that depends on its inertia λ, thereby determining $\tilde{r}_{p1}(\tilde{T})$. This phase shift causes a rectified, steady contribution to the particle velocity over an oscillation cycle. The combination of this inertial rectification and the steady transport flow yields a steady radial particle velocity, which in units of u_s reads

$$\frac{d\tilde{r}_{p0}}{d\tilde{T}} = \frac{\lambda \tilde{h}_0}{\tilde{h}_0 + \gamma}\left[\frac{\gamma(\tilde{h}_0 + 4\gamma)}{2(1 + \tilde{h}_0 + 4\gamma)^3}\,\frac{2\tilde{h}_0 + \gamma}{(\tilde{h}_0 + \gamma)^2 + \tilde{h}_0^2\lambda^2}\right] + \frac{\tilde{h}_0 \tilde{u}_L(\tilde{r}_{p0})}{\tilde{h}_0 + \gamma}, \tag{8}$$

where $\tilde{h}_0 = \tilde{r}_{p0} - 1 - 4\gamma$ is the average of the separation distance $\tilde{h}$ over an oscillation cycle, and $\tilde{u}_L = \tilde{\mathbf{u}}_L \cdot \mathbf{e}_r$.

The first term in Eq. (8) is due to the rectification of the particle's oscillatory inertia, while the second term represents radial transport by $\tilde{u}_L$, with a geometric factor accounting for the

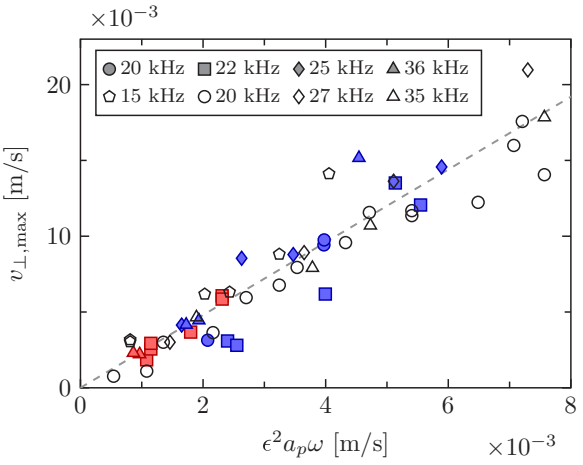

FIG. 4. Maximum normal velocity of particles $v_{\perp,\max}$ as a function of $\epsilon^2 a_p \omega$, showing experimental measurements (solid symbols) and simulation results (open symbols) for a variety of driving frequencies. Experimental data include particles of $a_p = 2.5\ \mu$m (red) and $a_p = 5\ \mu$m (blue), simulations cover a size range $0.5\ \mu\text{m} \leqslant a_p \leqslant 5\ \mu$m. The dashed line is the scaling prediction of (9) using $(-\partial\tilde{u}_L/\partial\tilde{r})_{\max,\tilde{r}=1} = 2.4$.

hydrodynamic resistance from the lubrication layer. The azimuthal motion corresponds to passive transport, so that the steady particle velocity approaches the steady fluid velocity $\tilde{\mathbf{u}}_L$ for $\tilde{h}_0 \gg \gamma$.

This monopole-only analytical simplification of the particle motion captures the salient features of the full trajectories. Note that oscillating bubbles, with dominant radial oscillations, are ideally suited experimental systems to study the accuracy of this approach. Consistent with both experiment and simulation, it demonstrates that the lift velocity $v_\perp$ is only appreciable when $\tilde{h}_0 \lesssim O(\gamma)$. Since steady fluid streamlines are nearly azimuthal close to the bubble surface, the particle velocity normal to the streamlines is approximately the radial velocity $\tilde{v}_\perp \approx d\tilde{r}_0/d\tilde{T} - \tilde{u}_L(\tilde{r}_{p0})$. Using a Taylor expansion to write $\tilde{u}_L \approx (\tilde{h}_0 + 4\gamma)(\partial\tilde{u}_L/\partial\tilde{r})|_{\tilde{r}=1}$, and assuming small separations ($\tilde{h}_0 \ll 1$) and particles much smaller than the bubble ($\gamma \ll 1$), we obtain

$$v_{\perp,\max} \approx \epsilon^2 a_p \omega \left(-\frac{\partial \tilde{u}_L}{\partial \tilde{r}}\bigg|_{\max} \right)_{\tilde{r}=1,} . \tag{9}$$

The quantity in parentheses represents the dimensionless maximum radial extensional shear rate of the steady flow near the bubble surface, for which analytical streaming theory [20] determines a mean value of ≈2.77 for f in the range 10–40 kHz.

The scaling $v_{\perp,\max} \propto \epsilon^2 a_p \omega$ predicted by (9) is confirmed across a range of amplitudes, frequencies, and particle sizes by experimental measurements as well as simulations (cf. Fig. 4). The best-fit prefactor is ≈2.4, close to the direct prediction from theory above. For the small particles used as passive-tracer proxies in the experiments, the expected displacement is below 1 μm, justifying this approximation. Note also that the hard-core steric interaction model of Ref. [16] predicts a particle displacement of a_p during a transport time near the bubble of order $1/(\epsilon^2\omega)$, i.e., this estimate is recovered as a limiting case if the displacement dynamics of the particle is dominated throughout by $v_{\perp,\max}$.

The present study provides quantitative measurements, as well as explicit modeling, of the inertial rectification of particle positions near oscillating boundaries. Here, the streaming flow induced by the same oscillations ensures particle transport, but the concept of inertial rectification is general—in fact, this type of particle displacement is even present in cases (such as purely radial oscillation) where no streaming is present. It is illuminating to compare the scaling of particle

velocities perpendicular to fluid pathlines with that in traditional shear-induced inertial particle migration. In the latter [4], a steady transport flow U in a channel of height H induces a lift velocity in the particle of order $v_{\dot{\gamma}} \sim U\lambda_{\dot{\gamma}}(a_p/H)^k$, where $\lambda_{\dot{\gamma}} = a_p^2 U/(H\nu)$ and $k = 1$ or $k = 3$ near the channel center or the channel wall, respectively. In comparison, the first term on the right-hand side of (8) represents a rectification velocity of (in dimensional terms) $v_R \sim u_s\lambda(a_p/a_b)$, in the relevant regime of $\lambda \lesssim 1$ and $\gamma \ll 1$. If we match the steady transport speeds in the two cases ($U = u_s$), we obtain $v_R/v_{\dot{\gamma}} \sim (H/\epsilon a_b)^2$ for $k = 1$, so that for typical experimental values the displacement speed utilizing the oscillating interface is three to four orders of magnitude greater (and this ratio becomes even larger for $k = 3$). These estimates show why particles get displaced highly effectively over millisecond time scales in our experiments. A direct comparison with acoustofluidic particle migration is inappropriate, as the present formalism is entirely incompressible, and the particles are density matched, so that acoustofluidic forces are zero. Further work will explore the effects on particles with a density mismatch.

The modeling approach successfully describes particle motion on all relevant time scales and captures its dependence on physical control parameters. The particular form of oscillatory flow used here is immaterial to the techniques employed; the effect of any periodic flow with appreciable particle inertia and extensional gradients can be understood analogously. The resulting rectified motion allows for fast targeted deflection and size segregation of micro- and nanoparticles, so that these insights provide inspiration for microfluidic devices capable of extremely rapid inertial particle manipulation.

The authors appreciate valuable discussions with J. F. Brady, S. H. Davis, G. Leal, M. Miksis, and D. Saintillan, and gratefully acknowledge support for this work by the National Science Foundation under Grant No. CBET-1236141.

[1] H. A. Stone and S. Kim, Microfluidics: basic issues, applications, and challenges, AIChE J. **47**, 1250 (2001).
[2] L. G. Leal, Particle motions in a viscous fluid, Annu. Rev. Fluid Mech. **12**, 435 (1980).
[3] D. Di Carlo, D. Irimia, R. G. Tompkins, and M. Toner, Continuous inertial focusing, ordering, and separation of particles in microchannels, Proc. Nat. Acad. Sci. USA **104**, 18892 (2007).
[4] D. Di Carlo, Inertial microfluidics, Lab Chip **9**, 3038 (2009).
[5] H. Bruus, Acoustofluidics 7: The acoustic radiation force on small particles, Lab Chip **12**, 1014 (2012).
[6] R. Barnkob, P. Augustsson, T. Laurell, and H. Bruus, Acoustic radiation- and streaming-induced microparticle velocities determined by microparticle image velocimetry in an ultrasound symmetry plane, Phys. Rev. E **86**, 056307 (2012).
[7] D. J. Collins, B. Morahan, J. Garcia-Bustos, C. Doerig, M. Plebanski, and A. Neild, Two-dimensional single-cell patterning with one cell per well driven by surface acoustic waves, Nat. Commun. **6**, 8686 (2015).
[8] P. Augustsson, J. T. Karlsen, H.-W. Su, H. Bruus, and J. Voldman, Iso-acoustic focusing of cells for size-insensitive acousto-mechanical phenotyping, Nat. Commun. **7**, 11556 (2016).
[9] G. A. Voth, B. Bigger, M. R. Buckley, W. Losert, M. P. Brenner, H. A. Stone, and J. P. Gollub, Ordered Clusters and Dynamical States of Particles in a Vibrated Fluid, Phys. Rev. Lett. **88**, 234301 (2002).
[10] H. A. Pacheco-Martinez, L. Liao, R. J. A. Hill, M. R. Swift, and R. M. Bowley, Spontaneous Orbiting of Two Spheres Levitated in a Vibrated Liquid, Phys. Rev. Lett. **110**, 154501 (2013).
[11] D. Klotsa, K. A. Baldwin, R. J. A. Hill, R. M. Bowley, and M. R. Swift, Propulsion of a Two-Sphere Swimmer, Phys. Rev. Lett. **115**, 248102 (2015).
[12] B. R. Lutz, J. Chen, and D. T. Schwartz, Hydrodynamic tweezers: 1. Noncontact trapping of single cells using steady streaming microeddies, Anal. Chem. **78**, 5429 (2006).
[13] P. Rogers and A. Neild, Selective particle trapping using an oscillating microbubble, Lab Chip **11**, 3710 (2011).
[14] Y. Chen, Z. Fang, B. Merritt, D. Strack, J. Xu, and S. Lee, Onset of particle trapping and release via acoustic bubbles, Lab Chip **16**, 3024 (2016).

[15] C. Wang, S. V. Jalikop, and S. Hilgenfeldt, Size-sensitive sorting of microparticles through control of flow geometry, Appl. Phys. Lett. **99**, 034101 (2011).
[16] R. Thameem, B. Rallabandi, and S. Hilgenfeldt, Particle migration and sorting in microbubble streaming flows, Biomicrofluidics **10**, 014124 (2016).
[17] N. Riley, Steady streaming, Annu. Rev. Fluid Mech. **33**, 43 (2001).
[18] M. Wiklund, R. Green, and M. Ohlin, Acoustofluidics 14: Applications of acoustic streaming in microfluidic devices, Lab Chip **12**, 2438 (2012).
[19] C. Wang, B. Rallabandi, and S. Hilgenfeldt, Frequency dependence and frequency control of microbubble streaming flows, Phys. Fluids **25**, 022002 (2013).
[20] B. Rallabandi, C. Wang, and S. Hilgenfeldt, Two-dimensional streaming flows driven by sessile semicylindrical microbubbles, J. Fluid Mech. **739**, 57 (2014).
[21] B. J. Davidson and N. Riley, Cavitation microstreaming, J. Sound Vib. **15**, 217 (1971).
[22] M. S. Longuet-Higgins, Viscous streaming from an oscillating spherical bubble, Proc. R. Soc. London, Ser. A **454**, 725 (1998).
[23] See Supplemental Material at http://link.aps.org/supplemental/10.1103/PhysRevFluids.2.052001 for videos of particle motion, as well as for detailed justifications of the theoretical formalism.
[24] H. Brenner, The slow motion of a sphere through a viscous fluid towards a plane surface, Chem. Eng. Sci. **16**, 242 (1961).
[25] R. H. Davis, J.-M. Serayssol, and E. J. Hinch, The elastohydrodynamic collision of two spheres, J. Fluid Mech. **163**, 479 (1986).
[26] M. R. Maxey and J. J. Riley, Equation of motion for a small rigid sphere in a nonuniform flow, Phys. Fluids **26**, 883 (1983).
[27] S. L. Dance and M. R. Maxey, Incorporation of lubrication effects into the force-coupling method for particulate two-phase flow, J. Comput. Phys. **189**, 212 (2003).
[28] B. Rallabandi, S. Hilgenfeldt, and H. Stone, Hydrodynamic force on a sphere normal to an obstacle due to a non-uniform flow, J. Fluid Mech. **818**, 407 (2017).
[29] T. N. Phung, J. F. Brady, and G. Bossis, Stokesian dynamics simulation of Brownian suspensions, J. Fluid Mech. **313**, 181 (1996).
[30] J. W. Swan and J. F. Brady, Simulation of hydrodynamically interacting particles near a no-slip boundary, Phys. Fluids **19**, 113306 (2007).
[31] A. Marin, M. Rossi, B. Rallabandi, C. Wang, S. Hilgenfeldt, and C. J. Kähler, Three-Dimensional Phenomena in Microbubble Acoustic Streaming, Phys. Rev. Appl. **3**, 041001 (2015).
[32] B. Rallabandi, A. Marin, M. Rossi, C. J. Kähler, and S. Hilgenfeldt, Three-dimensional streaming flow in confined geometries, J. Fluid Mech. **777**, 408 (2015).
[33] N.-Q. Nguyen and A. J. C. Ladd, Lubrication corrections for lattice-Boltzmann simulations of particle suspensions, Phys. Rev. E **66**, 046708 (2002).
[34] K. Chong, S. D. Kelly, S. Smith, and J. D. Eldredge, Inertial particle trapping in viscous streaming, Phys. Fluids **25**, 033602 (2013).
[35] C. M. Bender and S. A. Orszag, *Advanced Mathematical Methods for Scientists and Engineers I* (Springer, Berlin, 1999).